Optics Letters

Ultrafast light-driven magneto-optical nonlinearity in ferromagnetic heterostructures

Yexin Jiang,[1,†] Zhangshun Li,[1,†] Zhuoyi Li,[2,†] Zuanming Jin,[1,*] Xianyang Lu,[2] Yongbing Xu,[2] Yan Peng,[1] and Yiming Zhu[1]

[1] Terahertz Technology Innovation Research Institute, Terahertz Spectrum and Imaging Technology Cooperative Innovation Center, Shanghai Key Lab of Modern Optical System, University of Shanghai for Science and Technology, Shanghai 200093, China
[2] Jiangsu Provincial Key Laboratory of Advanced Photonic and Electronic Materials, School of Electronic Science and Engineering, Nanjing University, Nanjing 210093, China
[†] These authors contributed equally to this Letter.
*physics_jzm@usst.edu.cn

Received 18 January 2023; revised 18 March 2023; accepted 19 March 2023; posted 20 March 2023; published 6 April 2023

The dynamic control of magnetization by short laser pulses has recently attracted interest. The transient magnetization at the metallic magnetic interface has been investigated through second-harmonic generation and the time-resolved magneto-optical effect. However, the ultrafast light-driven magneto-optical nonlinearity in ferromagnetic heterostructures for terahertz (THz) radiation remains unclear. Here, we present THz generation from a metallic heterostructure, Pt/CoFeB/Ta, which is ascribed to an ~6–8% contribution from the magnetization-induced optical rectification and an ~94–92% contribution from both spin-to-charge current conversion and ultrafast demagnetization. Our results show that THz-emission spectroscopy is a powerful tool to study the picosecond-time-scale nonlinear magneto-optical effect in ferromagnetic heterostructures.

https://doi.org/10.1364/OL.485966

Second-order nonlinear optical processes are sensitive to the crystal lattice symmetry in solids [1]. On the one hand, surface second-harmonic generation due to a non-zero $\chi^{(2)}$ has been widely used to detect symmetry breaking on the surface [2,3]. On the other hand, optical rectification has been widely used for THz generation in bulk semiconductors, metallic surfaces, and interfaces with centrosymmetric breaking [4–6].

Generally, in the case of magnetic surfaces or interfaces, the presence of magnetization does not affect the bulk inversion symmetry but it does change the symmetry of the interface [7]. Magnetization-induced second-harmonic generation has been widely used to probe the structure and magnetism of ferromagnetic interfaces [8,9]. In addition, the time-resolved spin polarization can also be analyzed by optical second-harmonic generation [10,11]. Also, by means of magneto-optical pump-probe measurements with elliptically polarized light pumping, both ultrafast demagnetization and transient circular/linear birefringence can be observed in Ni and a magnetic ionic liquid [12–14]. The ultrafast polarization is induced by both the inverse Faraday effect and the optical Kerr effect. The inverse Faraday effect occurs due to transient magnetization, which is regarded as a magneto-optical rectification [15]. The optical Kerr effect is dominated by the cascading $\chi^{(2)}\cdot\chi^{(2)}$ contribution [16], which has been used to modulate the polarization of light at THz frequencies [17].

Recently, THz emission spectroscopy has been widely utilized as an efficient tool to study (1) the nonlinear emerging properties of topological materials, such as the photo-galvanic effect [18] and the photon drag effect [19], and (2) ultrafast demagnetization (UDM) [20,21] and spin-to-charge current conversion (SCC) in ferromagnetic (FM)/nonmagnetic metal (NM) heterostructures [22]. Nevertheless, there is still an open question of whether the magneto-optical nonlinear effect appearing at the interface of a FM/NM heterostructure plays a key role in THz generation [23,24]. Such knowledge is indispensable when investigating the interfacial physics [25] (symmetry breaking [26], surface roughness [27], band structure [28], topological Dirac state [29], and metal–insulator phase transition [30]) and optimizing spintronic THz emitters [31,32].

In this Letter, we investigate the broadband THz generation from an interface in the Pt/CoFeB/Ta heterostructure based on pump polarization and applied magnetic field dependent measurements. Our experimental results demonstrate that ~6–8% of the THz generation arises from the interface's magneto-optical nonlinearity, and the rest is contributed by both SCC and UDM. Our results not only clarify that interface magnetization-induced optical rectification is a nontrivial mechanism for THz generation, but they also raise the potential of THz emission spectroscopy to be applied to the investigation of interfacial nonlinear optics and physics.

All samples were deposited in multilayer stacks on single-crystalline MgO substrates via DC/radio-frequency (RF) magnetron sputtering at room temperature. The magnetron sputtering system was kept at a base pressure of 3×10^{-8} Torr. The multilayer stack on the MgO was sequenced as follows: Pt/CoFeB/Ta and Ta/CoFeB/Pt (the thickness of each layer was 2 nm). A sputtering power of DC 10 W was used for Pt and CoFeB, while DC 15 W was used for Ta (with Ar at a pressure of 7 mTorr). During deposition, the substrate was rotated at a

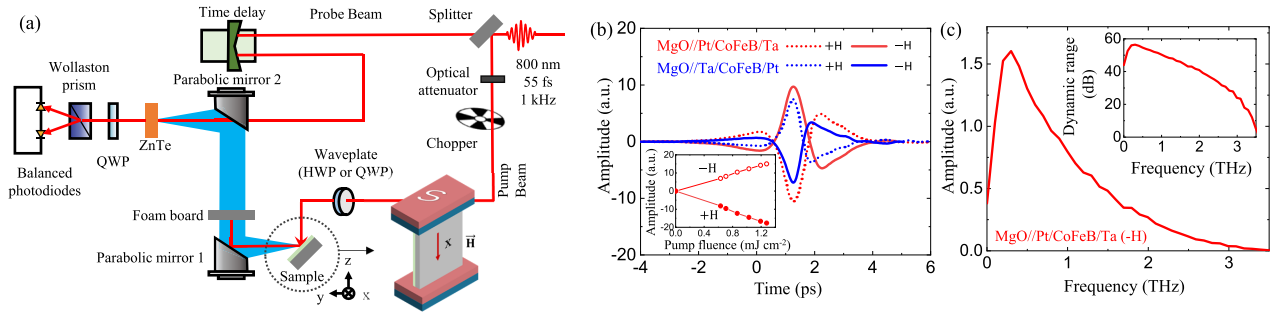

Fig. 1. Illustration of THz emission from a FM/NM surface with laser excitation. (a) Experimental schematic of THz-emission spectroscopy. The *xyz* coordinate is defined for the laboratory frame. (b) Observed THz EOS signals of MgO//Pt/CoFeB/Ta and MgO//Ta/CoFeB/Pt with ± **H** (along the *x* axis). Inset: the THz emission peak value as a function of pump fluence. (c) The frequency-domain spectrum of MgO//Pt/CoFeB/Ta with −**H**, as calculated by a fast Fourier transform. Inset: the corresponding dynamic range spectrum.

speed of 5 rpm. After deposition, the films were annealed *in situ* at 250°C for 60 minutes in vacuum in the absence of a magnetic field.

As shown in Fig. 1(a), the THz generation experiments were performed in the direction of specular reflection. The MgO//Pt/CoFeB/Ta sample was studied under irradiation homogeneously by an optical pulse (central wavelength 800 nm, pulse duration 55 fs, repetition rate 1 kHz). The surface normal of the sample was at incident angle of 45° with respect to the pump beam. The polarization of the incident pump beam was varied by using a half-wave plate (HWP) or a quarter-wave plate (QWP). The magnetization of the sample was set by applying an external magnetic field ($\mathbf{H} = 200$ mT) parallel to the x axis (in-plane) and perpendicular to the wave vector of the pump beam (−z-axis). The THz emission was collected by a parabolic mirror and detected by a 1-mm-thick <110> ZnTe crystal. The emitted THz amplitude and phase were detected with far-field free-space electro-optic sampling (EOS), employing the delay stage to vary the arrival time of the probe beam (55 fs, 800 nm) relative to the THz pulse. A chopper was used to modulate the pump beam with a frequency of 500 Hz. All the measurements were performed at room temperature. The THz-generating spectrometer was purged with dry air to avoid THz absorption by water vapor.

Figure 1(b) shows typical THz-emission EOS signals $E_{THz}^{EOS}(t)$ generated from MgO//Pt/CoFeB/Ta and MgO//Ta/CoFeB/Pt surfaces illuminated with p-polarized laser pulses (pump fluence 0.63 mJ cm^{-2}), from the metallic layer side. It is seen that, for each sample, the sign of the emitted THz traces reverses upon the reversal of **H**, confirming its magnetic origin. We chose Pt/CoFeB/Ta because Pt and Ta exhibit spin Hall angles with opposite signs. Because of this choice, the charge currents in the Pt and Ta layers flow in the same direction, radiate in phase, and boost the THz amplitude [21,31]. It can be seen that reversing the order of the Ta and Pt layers results in a reversal of the sign of the emitted THz waveforms. Thus, $E_{THz}^{Pt/CoFeB/Ta}(t) = E_{THz}^{UDM}(t) + E_{THz}^{SCC}(t)$ while $E_{THz}^{Ta/CoFeB/Pt}(t) = E_{THz}^{UDM}(t) - E_{THz}^{SCC}(t)$ when **H** is fixed. This is the reason why the THz generation from MgO//Pt/CoFeB/Ta is larger than that from MgO//Ta/CoFeB/Pt. All these observations are in accordance with the THz generation in the transmission configuration [33]. The THz emission process can be dominantly attributed to the SCC and partially to the UDM.

The inset in Fig. 1(b) shows a linear dependence of the THz emission peak value E_{THz}^{peak} on the pump fluence from 0.63 to 1.28 mJ cm^{-2}, below the damage threshold. The time-domain signals are shown in Note S1 in the Supplement 1. The level of THz emission from Pt/CoFeB/Ta is the same as that from a 1-mm-thick InP crystal surface (see Fig. S2), which is the main contribution to the surface-field effect [34]. The frequency-domain THz spectrum is shown in Fig. 1(c). The central frequency of the THz signal emitted from Pt/CoFeB/Ta is about 0.3 THz, with a frequency range of 0.1–3.0 THz. The inset of Fig. 1(c) shows that the peak dynamic range of the radiated THz pulse from Pt/CoFeB/Ta is around 57 dB.

In order to investigate the THz generation from the MgO//Pt/CoFeB/Ta heterostructure via the nonlinear magneto-optical effect, we measured the linear pump polarization dependence of $E_{THz}^{EOS}(t)$ by rotating the HWP. The angle θ_P characterizes the linear-polarization state with respect to the p-polarized pump pulse ($\theta_P = 0°$). As indicated by the black dashed-dotted curves in Fig. 2(a), the peak amplitude of the THz emission exhibits a periodic oscillation with the variation of θ_P. Figure 2(b) shows that E_{THz}^{peak} varies with θ_P. The solid circles and hollow circles represent the experimental results obtained with + **H** and −**H**, respectively. E_{THz}^{peak} is composed of a pump-polarization-independent isotropic term (dashed line) and a pump-polarization-dependent anisotropic term (dotted line). The sign of the isotropic component flips after the **H** is reversed, as shown by the red and blue dashed lines. As the reversal of the magnetic field leads to the opposite directions of both the magnetization and the spin-to-charge current conversion [21,31–33], it confirms that both the SCC and the UDM are components of the isotropic termthe isotropic term.

To further investigate the mechanism of the anisotropic term, we measured the dependence of E_{THz}^{peak} on the helicity of the pump pulse, which was controlled by rotating a QWP. Figure 3(a) shows the E_{THz}^{peak} dependence on the QWP angle φ with a periodicity of $\pi/2$. $E_{THz}^{peak}(\varphi)$ does not show any periodicity of π. As shown in Fig. 3(b), the $E_{THz}^{EOS}(t)$ induced by left circularly polarized pumping (LCP) is very similar to that generated by right circularly polarized pumping (RCP). These experimental results demonstrate that the modulation of THz emission by the polarization state mainly comes from the linear polarization of the pump beam. This result is quite different from GaAs, where the THz emission is helicity dependent, which can be explained by the spin-polarized electrons [35,36]. Meanwhile, the inverse Faraday effect and the circular photo-galvanic effect can also be excluded, as the possible manipulation of the light-driven

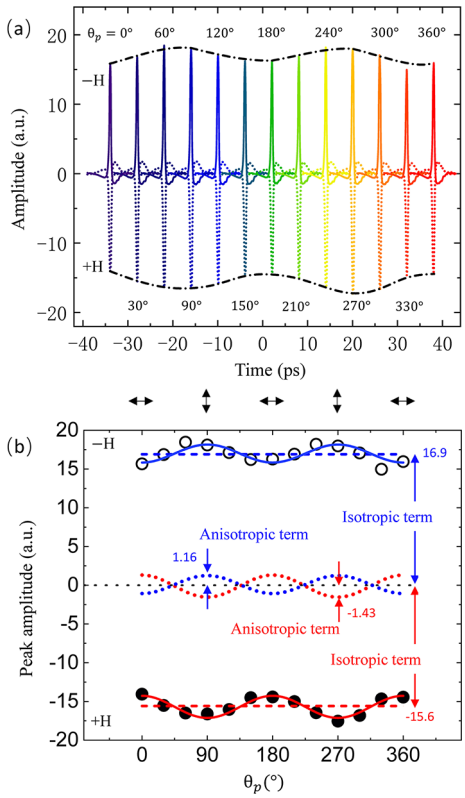

Fig. 2. THz emission from MgO//Pt/CoFeB/Ta with different linearly polarized pumping under ± **H**. (a) $E_{THz}^{EOS}(t)$ measured at various θ_P. For clarity, all $E_{THz}^{EOS}(t)$ are shifted horizontally according to the θ_P. (b) E_{THz}^{peak} (circles) measured as functions of θ_P for ± **H**. The solid curves are fits obtained using Eq. (5).

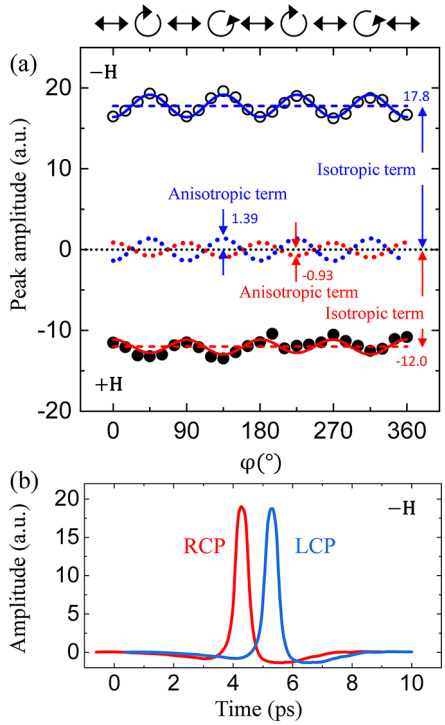

Fig. 3. THz emission variation with different elliptically polarized pumping. (a) E_{THz}^{peak} as a function of φ (circles). The pump beam was p-polarized when $\varphi = 0°, 90°, 180°, 270°, 360°$, circularly polarized when $\varphi = 45°, 135°, 225°, 315°$, and elliptically polarized at intermediate degrees. The solid curves are fits obtained using Eq. (6). (b) Typical measured $E_{THz}^{EOS}(t)$ values induced by RCP and LCP (offset horizontally).

ultrafast polarization and injection current are helicity dependent [37,38]. Therefore, the anisotropic term can be assigned to nonlinear optical rectification.

Upon femtosecond laser excitation, a rapid change of second-order nonlinear polarization can be induced:

$$P_{OR}^{(2)}(\Omega) = \varepsilon_0 \chi^{(2)}(\Omega, \omega + \Omega, \ -\omega) E(\omega + \Omega) E^*(\omega), \quad \textbf{(1)}$$

where $E(\omega)$ is the electric field of the incident pump beam. ω and Ω are the optical frequency and THz frequency, respectively. The second-order susceptibility has the general form

$$\chi^{(2)} = \chi_{structure}^{(2)} + \chi_{magnetization}^{(2)} \quad \textbf{(2)}$$

where $\chi_{structure}^{(2)}$ describes the interface with centrosymmetric breaking. The second term represents the magnetic component, $\chi_{magnetization}^{(2)} \propto \chi_{structure}^{(2)} \cdot \mathbf{M}$, which is nonzero in the presence of centrosymmetric breaking. Based on the second-order optical process, $E_{THz}(t) \propto \frac{\partial^2 P_{OR}^{(2)}(t)}{\partial t^2}$. The relationship between the THz emission signal and the polarization state of the pump pulse can be described as (see Note S3 of the Supplement 1) [39]

$$E_{THz}(\theta_P) \propto I_{pump} \cdot \chi^{(2)} \cdot \cos(2\theta_P) \text{(Linearly Polarized pumping)} \quad \textbf{(3)}$$

$$E_{THz}(\varphi) \propto I_{pump} \cdot \chi^{(2)} \cdot \cos(4\varphi) \text{ (Circularly Polarized pumping)} \quad \textbf{(4)}$$

where I_{pump} is the intensity of the pump beam. Thus, the peak amplitude of the generated THz can be fitted by the functions

$$E_{THz}^{peak}(\theta_P) = A_i + A_{ani} \cdot \cos(2\theta_P) \text{ (Linearly Polarized pumping)} \quad \textbf{(5)}$$

$$E_{THz}^{peak}(\varphi) = A_i + A_{ani} \cdot \cos(4\varphi) \text{ (Circularly Polarized pumping)} \quad \textbf{(6)}$$

where A_i refers to the amplitude of the isotropic term, which mainly comes from SCC and UDM, and A_{ani} represents the anisotropic term. Using Eq. (5) and Eq. (6), respectively, we can fit the data in Fig. 2(b) and Fig. 3(a) very well (solid curves). The dashed lines are the fitted A_i for + **H** (red) and −**H** (blue), while the dotted lines are the fitted cosine terms for + **H** (red) and −**H** (blue). It is important to note that the pump-polarization-dependent terms flip over when the external magnetic field is reversed. This result indicates that the dominant contribution to $\chi^{(2)}$ comes from $\chi_{magnetization}^{(2)}$. Since the absolute values of anisotropic terms are not exactly identical under opposite magnetic fields, this means that the structurally induced centrosymmetric breaking cannot be negligible.

The contribution ratio of the anisotropic term can be defined as $\rho = |A_{ani}|/(|A_i| + |A_{ani}|)$, where $|A_{ani}|$ and $|A_i|$ are obtained from the fitting curves in Fig. 2(b) and Fig. 3(a). Thus, for our Pt/CoFeB/Ta trilayer, ρ = 8.4 % (+**H**) and 6.4% (−**H**) for Linearly Polarized pumping and 7.2 % (±**H**) for Circularly Polarized pumping. These values are smaller than the contribution ratio of ~35% observed in bilayers of the Heusler alloy CoFeMnSi/Pd [40]. Note that since there is no rigorous reconstruction of the THz electric and/or magnetic dipole field

[21], the contribution proportions of the surface magneto-optical nonlinearity, SCC, and UDM mechanism to the THz emission are only approximate. Therefore, a comprehensive experimental reconstruction [41] and theoretical treatment [42] are required to elucidate their exact THz temporal dynamics.

In conclusion, we have investigated the THz emission from a Pt/CoFeB/Ta heterostructure. We find that part of the amplitude of THz emission (~6-8%) depends on the polarization of the pump beam. In particular, the polarity of pump-polarization-dependent THz emission depends on the magnetization orientation, which is in accordance with the surface-magnetization-induced optical rectification. In future work, more surface annealing and a doping treatment could be adopted to tune the magneto-optical nonlinearity. Moreover, this surface engineering could in turn be used as a novel manipulation method for spintronic THz emitters.

Funding. National Natural Science Foundation of China (61975110, 61988102, 12204216, 61427812, 12104216); 111 Project (D18014); the Key project supported by Science and Technology Commission Shanghai Municipality (YDZX20193100004960); Science and Technology Commission of Shanghai Municipality (22JC1400200); General Administration of Customs People's Republic of China (2019HK006); Natural Science Foundation of Jiangsu Province (BK20200307); National Key Research and Development Program of China (2021YFB3601600).

Disclosures. The authors declare no conflicts of interest.

Data availability. Data underlying the results presented in this paper are not publicly available at this time but may be obtained from the authors upon reasonable request.

Supplemental document. See Supplement 1 for supporting content.

REFERENCES

1. Y. R. Shen, *The Principles of Nonlinear Optics*, John Wiley & Sons (1984).
2. R.-P. Pan, H. D. Wei, and Y. R. Shen, Phys. Rev. B **39**, 1229 (1989).
3. J. Reif, J. C. Zink, C.-M. Schneider, and J. Kirschner, Phys. Rev. Lett. **67**, 2878 (1991).
4. X.-C. Zhang, Y. Jin, K. Yang, and L. J. Schowalter, Phys. Rev. Lett. **69**, 2303 (1992).
5. J. A. Fülöp, S. Tzortzakis, and T. Kampfrath, Adv. Opt. Mater. **8**, 1900681 (2020).
6. I. Nevinskas, K. Vizbaras, A. Trinkūnas, R. Butkutė, and A. Krotkus, Opt. Lett. **42**, 2615 (2017).
7. S. L. Chuang, S. Schmitt-Rink, B. I. Greene, P. N. Saeta, and A. F. J. Levi, Phys. Rev. Lett. **68**, 102 (1992).
8. Y. Ogawa, Y. Kaneko, J. P. He, X. Z. Yu, T. Arima, and Y. Tokura, Phys. Rev. Lett. **92**, 047401 (2004).
9. A. Kirilyuk and T. Rasing, Appl. Phys. Lett. **72**, 2331 (1998).
10. A. Melnikov, I. Razdolski, T. O. Wehling, E. T. Papaioannou, V. Roddatis, P. Fumagalli, O. Aktsipetrov, A. I. Lichtenstein, and U. Bovensiepen, Phys. Rev. Lett. **107**, 076601 (2011).
11. A. Alekhin, I. Razdolski, N. Ilin, J. P. Meyburg, D. Diesing, V. Roddatis, I. Rungger, M. Stamenova, S. Sanvito, U. Bovensiepen, and A. Melnikov, Phys. Rev. Lett. **119**, 017202 (2017).
12. P. J. Bennett, V. Albanis, Y. P. Svirko, and N. I. Zheludev, Opt. Lett. **24**, 1373 (1999).
13. R. Wilks, R. J. Hicken, M. Ali, B. J. Hickey, J. D. R. Buchanan, A. T. G. Pym, and B. K. Tanner, J. Appl. Phys. **95**, 7441 (2004).
14. Z. Jin, H. Ma, D. Li, G. Ma, M. Wang, and C. Zhao, J. Appl. Phys. **109**, 073109 (2011).
15. R. V. Mikhaylovskiy, E. Hendry, and V. V. Kruglyak, Phys. Rev. B **86**, 100405 (2012).
16. T. Suzuki, R. Mondal, Y. Saito, P. Fons, A. V. Kolobov, J. Tominaga, H. Shigekawa, and M. Hase, J. Phys.: Condens. Matter **31**, 415502 (2019).
17. R. R. Subkhangulov, R. V. Mikhaylovskiy, A. K. Zvezdin, V. V. Kruglyak, T. Rasing, and A. V. Kimel, Nat. Photonics **10**, 111 (2016).
18. Y. Gao, S. Kaushik, E. J. Philip, Z. Li, Y. Qin, Y. P. Liu, W. L. Zhang, Y. L. Su, X. Chen, H. Weng, D. E. Kharzeev, M. K. Liu, and J. Qi, Nat. Commun. **11**, 720 (2020).
19. L. Cheng, Y. Xiong, L. Kang, Y. Gao, Q. Chang, M. Chen, J. Qi, H. Yang, Z. Liu, J. C. W. Song, and E. M. Chia, Sci. Adv. **9**, eadd7856 (2023).
20. S. Zhang, Z. Jin, X. Liu, W. Zhao, X. Lin, C. Jing, and G. Ma, Opt. Lett. **42**, 3080 (2017).
21. W. Zhang, P. Maldonado, Z. Jin, T. S. Seifert, J. Arabski, G. Schmerber, E. Beaurepaire, M. Bonn, T. Kampfrath, P. M. Oppeneer, and D. Turchinovich, Nat. Commun. **11**, 4247 (2020).
22. T. Kampfrath, M. Battiato, P. Maldonado, G. Eilers, J. Nötzold, S. Mährlein, V. Zbarsky, F. Freimuth, Y. Mokrousov, S. Blügel, M. Wolf, I. Radu, P. M. Oppeneer, and M. Münzenberg, Nat. Nanotechnol. **8**, 256 (2013).
23. D. J. Hilton, R. D. Averitt, C. A. Meserole, G. L. Fisher, D. J. Funk, J. D. Thompson, and A. J. Taylor, Opt. Lett. **29**, 1805 (2004).
24. N. Kumar, R. W. A. Hendrikx, A. J. L. Adam, and P. C. M. Planken, Opt. Express **23**, 14252 (2015).
25. W. Du, Y. Huang, Y. Zhou, and X. Xu, J. Phys. D: Appl. Phys. **55**, 223002 (2022).
26. Q. Zhang, Z. Luo, H. Li, Y. Yang, X. Zhang, and Y. Wu, Phys. Rev. Appl. **12**, 054027 (2019).
27. O. Gueckstock, L. Nádvorník, M. Gradhand, T. S. Seifert, G. Bierhance, R. Rouzegar, M. Wolf, M. Vafaee, J. Cramer, M. A. Syskaki, G. Woltersdorf, I. Mertig, G. Jakob, M. Kläui, and T. Kampfrath, Adv. Mater. **33**, 2006281 (2021).
28. Z. Jin, Y. Guo, Y. Peng, Z. Zhang, J. Pang, Z. Zhang, F. Liu, B. Ye, Y. Jiang, G. Ma, C. Zhang, A. V. Balakin, A. P. Shkurinov, Y. Zhu, and S. Zhuang, Adv. Phys. Res. **2**, 2200049 (2023).
29. H. Park, S. Rho, J. Kim, H. Kim, D. Kim, C. Kang, and M.-H. Cho, Adv. Sci. **9**, 2200948 (2022).
30. M. Esaulkov, P. Solyankin, A. Sidorov, L. Parshina, A. Makarevich, Q. Jin, Q. Luo, O. Novodvorsky, A. Kaul, E. Cherepetskaya, A. Shkurinov, V. Makarov, and X.-C. Zhang, Optica **2**, 790 (2015).
31. T. Seifert, S. Jaiswal, and U. Martens, *et al.*, Nat. Photonics **10**, 483 (2016).
32. Z. Jin, Y. Peng, Y. Ni, G. Wu, B. Ji, X. Wu, Z. Zhang, G. Ma, C. Zhang, L. Chen, A. V. Balakin, A. P. Shkurinov, Y. Zhu, and S. Zhuang, Laser Photonics Rev. **16**, 2100688 (2022).
33. Z. Li, Y. Jiang, Z. Jin, Z. Li, X. Lu, Z. Ye, J. Pang, Y. Xu, and Y. Peng, Nanomaterials **12**, 4267 (2022).
34. P. Cicėnas, A. Geižutis, V. L. Malevich, and A. Krotkus, Opt. Lett. **40**, 5164 (2015).
35. J. M. Schleicher, S. M. Harrel, and C. A. Schmuttenmaer, J. Appl. Phys. **105**, 113116 (2009).
36. F. Nastos, R. W. Newson, J. Hübner, H. M. van Driel, and J. E. Sipe, Phys. Rev. B **77**, 195202 (2008).
37. Z. Ni, K. Wang, Y. Zhang, O. Pozo, B. Xu, X. Han, K. Manna, J. Paglione, C. Felser, A. G. Grushin, F. de Juan, E. J. Mele, and L. Wu, Nat. Commun. **12**, 154 (2021).
38. S. Ruan, X. Lin, H. Chen, B. Song, Y. Dai, X. Yan, Z. Jin, G. Ma, and J. Yao, Appl. Phys. Lett. **118**, 011102 (2021).
39. Y. Gao, Y. Pei, T. Xiang, L. Cheng, and J. Qi, iScience **25**, 104511 (2022).
40. Z. Yao, H. Fu, W. Du, Y. Huang, Z. Lei, C. You, and X. Xu, Phys. Rev. B **103**, L201404 (2021).
41. W. Zhang and D. Turchinovich, Opt. Express **29**, 24411 (2021).
42. J. Wang, B.-F. Zhu, and R.-B. Liu, Phys. Rev. Lett. **104**, 256601 (2010).